RSC Sustainability

ROYAL SOCIETY OF CHEMISTRY

PAPER

View Article Online
View Journal | View Issue

Cite this: *RSC Sustainability*, 2025, **3**, 5225

Glycerol-derived ionic liquids: a new family of high-potential renewable ionic solvents

Sara Gracia-Barberán, [ab] Jesús del Barrio, [ac] Alejandro Leal-Duaso, [ab] José A. Mayoral [ab] and Elísabet Pires *[ab]

Received 1st June 2025
Accepted 14th September 2025

DOI: 10.1039/d5su00393h

rsc.li/rscsus

This study describes a new family of bio-based ionic liquids (ILs) derived from glycerol, designed to address the environmental and toxicity concerns associated with conventional ILs. Two synthetic routes, starting from glycidyl ethers or epichlorohydrin are proposed in order to obtain a series of [N_20R]X ILs with varying alkyl chains (R) and anions (X^-), including chloride, triflate, bistriflimide, formate, and lactate. Comprehensive characterization of the ILs has been carried out, revealing tunable physicochemical properties, such as density (1.03–1.40 g cm^{-3}), viscosity (0.3–189 Pa s), and thermal stability (up to 672 K), influenced by structural modifications. The ILs demonstrated their applicability in two key applications: solubilizing hydroxycinnamic acids outperforming traditional solvents, and serving as recyclable media for Pd nanoparticle-catalyzed Heck–Mizoroki coupling, achieving quantitative yields and selectivity. These glycerol-derived ILs combine sustainability with functionality, offering a versatile platform for green chemistry applications.

Sustainability spotlight

This research advances sustainable chemistry by introducing a novel family of bio-based ionic liquids (ILs) derived from glycerol, a renewable feedstock, mitigating the environmental and toxicity risks of conventional ILs. Aligning with UN SDGs 12 (Responsible Consumption and Production) and 9 (Industry, Innovation, and Infrastructure), these ILs showcase tunable properties for green applications, including efficient solubilization of bioactive compounds and recyclable catalytic media for cross-coupling reactions. Their design reduces reliance on hazardous solvents (SDG 3: Good Health and Well-being) while enabling energy-efficient processes (SDG 7: Affordable and Clean Energy). By offering a non-toxic, biodegradable alternative with high functionality, this work supports circular economy principles (SDG 13: Climate Action) and promotes sustainable industrial innovation, bridging green chemistry with real-world applications.

1 Introduction

In recent decades, ionic liquids (ILs) have garnered significant attention across various fields of science and technology due to their exceptional properties, such as low volatility, thermal stability, and ability to dissolve a wide range of compounds, metals and ions.[1,2] In particular, these solvents have found applications in areas ranging from catalysis to the synthesis of organic compounds and advanced materials, establishing themselves as a promising alternative to conventional solvents.[3]

However, despite their advantages, traditional ILs present certain drawbacks. One of the major concerns is their toxicity and environmental impact, which has been well-documented in the literature.[4–6] For instance, the toxicity of ILs has been proved to vary depending on their structure, but many of them are harmful to aquatic environments and may pose significant risks if not handled correctly. In addition to the toxicity, issues such as high production costs, a limited purity, challenges in biodegradation and environmental fate concerns have imposed limitations on their long-term use.[7,8]

In response to these disadvantages, deep eutectic solvents (DES) emerged as a more accessible, benign and versatile alternative.[9,10] These mixtures offer a wide variety of chemical combinations, leading to a broad range of physicochemical properties. DES have been profusely used as reaction media in catalysis,[11] biorefinery processes,[12] preparation of materials,[13] or electrochemical applications,[14] among others. Nevertheless, one of the main limitations of DES is the potential separation of their components, which affects their stability and homogeneity in critical applications.[15]

To overcome these challenges, bio-based ionic liquids have recently emerged as an innovative and sustainable solution.[16–19] Unlike their traditional counterparts, bio-based ILs are composed of materials derived from renewable sources, such as amino acids,[20] sugars,[21–23] choline,[20,24,25] or glycerol,[26,27] improving both their environmental profile, biodegradability and biocompatibility. These liquids exhibit unique properties,

[a]*Departamento de Química Orgánica, Facultad de Ciencias, Universidad de Zaragoza, Calle Pedro Cerbuna, 12, E-50009 Zaragoza, Spain*

[b]*Instituto de Síntesis Química y Catálisis Homogénea (ISQCH), CSIC-Universidad de Zaragoza, Calle Pedro Cerbuna, 12, E-50009 Zaragoza, Spain*

[c]*Instituto de Nanociencia y Materiales de Aragón (INMA), CSIC-Universidad de Zaragoza, Calle Pedro Cerbuna, 12, Zaragoza, E-50009, Spain*

making them particularly attractive in applications,[19] such as solubilization of difficult compounds,[28] chiral recognition,[29,30] and catalysis.[31–33] Recent advancements in the synthesis of bio-based ILs have further highlighted their potential to reduce the environmental footprint, while maintaining the efficacy of traditional ILs. Additionally, their use in green chemistry has been emphasized as a critical step towards more sustainable industrial processes.[34]

Despite what has been described so far in the literature, there is a need for a portfolio of bio-based ionic liquids in which their physicochemical properties can be tuned on the basis of a common structure. Therefore, in this work we focus on the development of a new family of ionic liquids derived from glycerol platform molecules, with a wide range of physical-chemical properties that lead to high-potential applications including solubilisation and catalytic processes.

In this line, the development of a new family of solvents should be considered not only to provide the scientific community with new compounds with different properties, but also to prove its feasibility in applications of interest. Here, as a proof of concept, two applications have been envisaged for the developed ionic liquids. The first one is devoted to the solubilisation of products of interest, namely hydroxycinnamic acids. The second one consists of the use of these solvents for the design of recoverable active catalytic systems based on Pd nanoparticles.

2 Results and discussion

First, the synthesis of the new family of bio-based ionic liquids was addressed. These ILs are based on the C_3 structure of glycerol, with an ether alkyl chain (R) in position 3, and a *N*,*N*,*N*-triethylammonium group at position 1 ([N_20R]X, Fig. 1).

Triethylamine was selected as it is the smallest amine being a liquid, bringing practical handling benefits that facilitates the synthesis of aprotic ILs with small alkyl chains in the ammonium moiety.

A series of ILs varying the R substituents and anions (X^-) have been prepared and characterized.

This work proposes two distinct synthetic routes for the preparation of ionic liquids derived from glycerol. The first strategy employs glycidyl ethers as the starting material, while the second strategy involves two consecutive reaction steps from epichlorohydrin. Both platform molecules are available from bioglycerol and guarantee a much better reaction selectivity than starting from glycerol, thus improving the synthesis sustainability.

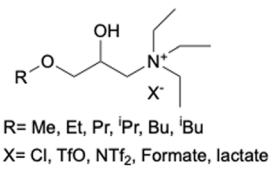

Fig. 1 General structure of the synthesized [N_20R]X ILs.

2.1 Synthesis of glycerol-derived ionic liquids from glycidyl ethers

This first strategy is inspired by the work of Xu *et al.*,[35] in which the synthesis of triple ammonium salts was addressed.

As shown in Scheme 1, this route involves the ring opening reaction of the epoxide of the corresponding glycidyl ether by triethylamine in acidic medium. Brønsted acidity was essential for the activation of the epoxide.

In the absence of a Brønsted acid, the epichlorohydrin opening reaction does not progress, thus it is clear that the acid may play a catalytic role increasing the electrophilic character of the epoxide carbon. However even in the absence of this role, the Brønsted acid shifts the equilibrium of the intermediate zwitterion towards the final products.

All of the reaction parameters were optimized using the methyl ether derivative as the benchmark reagent. The first reaction parameter to be optimized was the temperature. Two different temperatures were studied, 50 and 80 °C. As it can be seen in Table 1 (entries 2 and 3), the optimal temperature for the synthesis of the IL is 80 °C, with [N_201]Cl isolated yields above 70%.

Different reaction times (entries 1, 2 and 4) and triethylamine excesses (entries 3 and 5) were also tested and it was concluded that 48 hours and 50% of excess seemed to be the optimum reaction time at 80 °C, in a compromise between yield and reaction time.

In addition to the formation of the desired ammonium salt, when the reaction is analysed by ^{1}H NMR, the presence of two by-products is observed: triethylammonium chloride, formed by reaction of triethylamine with hydrochloric acid, and 1-chloro-3-methoxypropan-2-ol (**10Cl**), which is produced by the opening of the epoxide by the chloride anion (Scheme 1). As

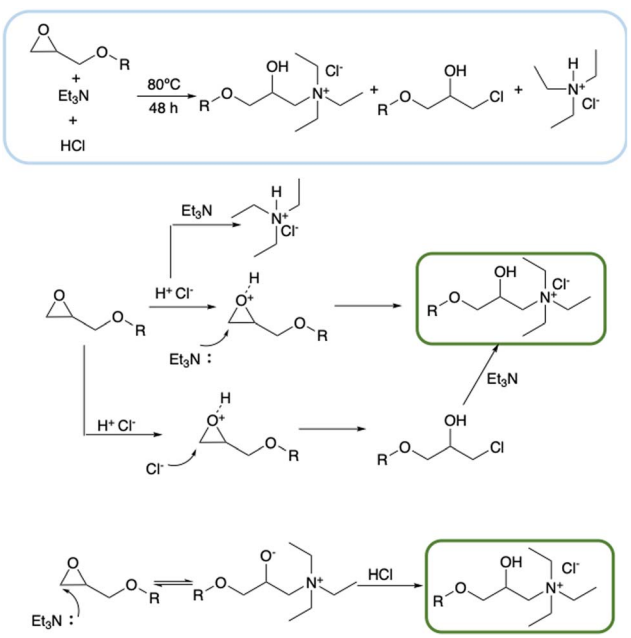

Scheme 1 Synthesis of ammonium salts-based ILs starting from glycidyl ethers.

Table 1 Conditions and yields for the synthesis from glycidyl methyl ether

Entry	Temperature (°C)	Time (h)	$[N_201]Cl$ yield[a] (%)	**R0Cl** yield[a] (%)	$NHEt_3Cl$ yield[a] (%)
1[b]	80	24	46	35	19
2[b]	50	48	33	40	27
3[b]	80	48	70	22	8
4[b]	80	72	75	13	12
5[c]	80	48	82	17	1

[a] Yields determined by ^{1}H NMR. [b] Reaction conditions: 5 mmol glycidyl methyl ether, 5 mmol HCl, 5 mmol Et_3N, rate of addition HCl:ether = 1/6. [c] 5 mmol glycidyl methyl ether, 5 mmol HCl, 7.5 mmol Et_3N.

shown in the Table 1, the rate of **R0Cl** formation decreases as the reaction time increases. This is due to the fact that as the reaction time progresses, the **R0Cl** reacts as well with the triethylamine by chlorine substitution, forming the desired ionic liquid. With regard to the formation of triethylammonium chloride salt, it seems to be erratic for different reaction times.

In order to minimize the formation of these side products, the addition of the reagents was optimized. It was noted that when all the reagents were added simultaneously to the reaction flask, the yield decreased significantly with respect to a controlled slow addition of both the acid and the ether.

2.2 Synthesis of glycerol-derived ionic liquids from epichlorohydrin

Although good results have been obtained in the aforementioned strategy, due to the high cost and the commercial availability of the glycidyl ethers, an alternative route was sought. As shown in Scheme 1, starting from glycidyl ethers, **R0Cl** is formed and subsequently transformed into the desired product by substitution of the chlorine atom with triethylamine. Therefore, the synthesis of the glycerol-derived ionic liquids was studied through the direct substitution reaction of chlorine in **R0Cl**. This **R0Cl** was previously obtained from epichlorohydrin, a renewable platform molecule derived from glycerol. This strategy involves two reaction steps. The first step is based on the preparation of **R0Cl** from the epichlorohydrin epoxide opening with an alcohol using a heterogeneous catalyst, montmorillonite K10.[36] This synthesis had previously been optimized and **R0Cl** yields of 98–89% were obtained, depending on the alcohol. It is noteworthy that, in addition to the desired **R0Cl** product, the formation of 2-alkoxy-3-chloro-1-propanol (**0RCl**) was observed during the course of the reactions. This by-product is formed by the attack of the alcohol on the most substituted position of the epichlorohydrin. Nevertheless, the formation of this compound is extremely rare in all cases, as the presence of a neighbouring chlorine atom in epichlorohydrin significantly impedes the reaction.

Once the **R0Cl** has been formed, it is reacted with triethylamine in order to carry out the chlorine substitution, to obtain the final product ($[N_20R]Cl$). In order to favour the reaction progress, a supply of 50% equivalents of triethylamine every 48 hours is needed (Scheme 2). In addition to the formation of the desired ionic liquid, the formation of

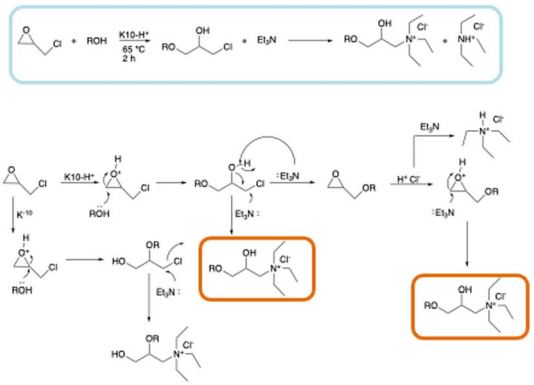

Scheme 2 Reaction pathways for the synthesis of ionic liquids from epichlorohydrin.

triethylammonium chloride salt was also observed. This salt can be generated by reaction of triethylamine and HCl. This HCl is *in situ* formed when a triethylamine molecule removes the hydrogen from the hydroxyl group of **R0Cl**, also resulting in the formation of the corresponding glycidyl ether (Scheme 2).

Again, several reaction parameters were optimized such as temperature, reaction time, and the use of a solvent in the second reaction step. To optimize the parameters, 1-chloro-3-methoxy-propan-2-ol (**10Cl**) has been used as the test compound. Table 2 gathers the yields of the ionic derivatives obtained in each case.

Table 2 Conditions and yields for the reaction of 1-chloro-3-methoxypropan-2-ol (**10Cl**) with triethylamine[a]

Entry	Time (h)	Temperature (°C)	Solvent	$[N_201]Cl$ yield[b] (%)
1	24	80	Solvent-free	16
2	24	100	Solvent-free	25
3	72	100	Solvent-free	40
4	120	100	Solvent-free	65
5	120	100	Solvent-free	52[c]
6	168	100	Solvent-free	79
7	120	100	Acetonitrile	25
8	168	100	Acetonitrile	40

[a] Reaction conditions: 0.3 mol **10Cl**, 0.3 mol Et_3N, 0.3 mol Et_3N refill every 48 h, dropwise addition of **10Cl**. [b] $[N_201]Cl$ yields calculated by ^{1}H NMR. [c] Simultaneous addition of **10Cl** and Et_3N.

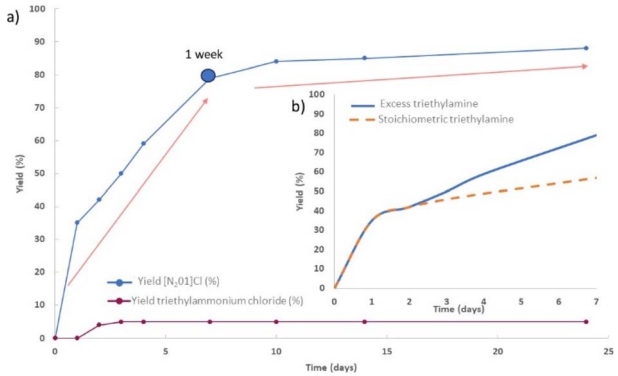

Fig. 2 (a) Ionic liquid yields over time. (b) Influence of the amount of Et_3N.

As expected, a higher temperature favours the reaction progress (Table 2, entries 1 and 2). A longer reaction time also increases the yield, the best results being obtained when the reaction is maintained for 1 week (168 h) (Table 2, entries 2–5 and Fig. 2). Finally, the use of a co-solvent did not seem to improve the results. When comparing the yields in the reactions with acetonitrile with the solventless reactions (Table 2, entries 4 and 7 or 6 and 8), it can be observed that notably higher yields are obtained in the case of the solvent-free reaction. Furthermore, the addition of both reagents simultaneously resulted in a significant reduction in yield compared to the controlled addition of **R0Cl** (Table 2, entry 5 *vs.* 4).

In view of these results, the reaction was monitored over time within the optimized conditions to evaluate both the evolution of the yield of the desired IL and the formation of the by-product triethylammonium chloride (Fig. 2).

As can be seen from the above graph, the reaction yield towards the desired ionic liquid increases with time. However, two distinct trends can be discerned. The first one exhibits a markedly steep slope up to seven reaction days, while the second displays a considerably more gradual slope. This is why 7 days (168 h) has been considered as the optimal reaction time, as from this point onwards the reaction slows down and the energy expenditure no longer compensates the yield obtained. Furthermore, it is observed that the formation of the triethylammonium chloride salt (Et_3NHCl) occurs during the first day of the reaction and remains constant during the following days, not exceeding in most cases the 5%.

As mentioned above, it is necessary to feed the reaction with an excess of triethylamine (50%) every 48 h. A study was carried out comparing the yields obtained with and without Et_3N refilling. As it can be seen in Fig. 2b, the yields are considerably higher when an excess of triethylamine is added. At the end of the reaction, the triethylamine : **R0Cl** molar ratio is 2.

Taking into account the above factors, the optimal conditions for the synthesis of $[N_20R]Cl$ ionic liquids from **R0Cl** are a temperature of 100 °C, a reaction time of seven days in the absence of additional solvent, and the addition of 50% excess triethylamine (with respect to the initial amount) every 48 hours.

Once the optimal reaction conditions were established, it was necessary to design a protocol for the purification of the

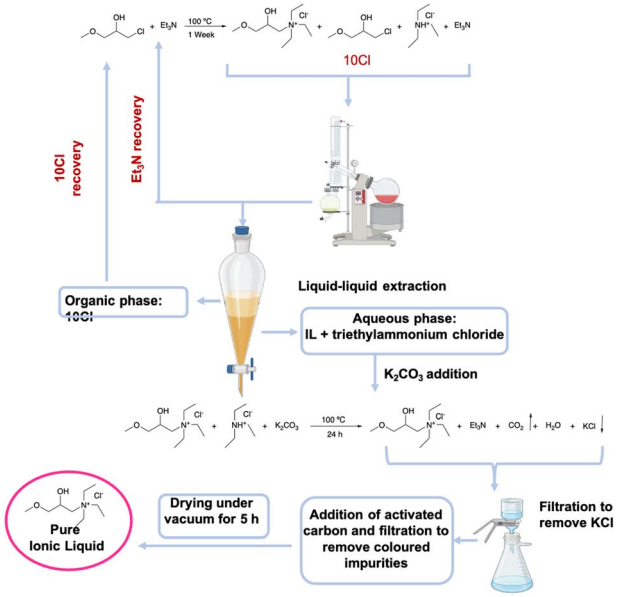

Scheme 3 Purification process of $[N_20R]Cl$ ionic liquids.

ionic liquid. ILs purification was a challenge due to the formation of by-products (Et_3NHCl) or the presence of starting materials (Et_3N and **R0Cl**). In order to optimize the synthesis from a sustainable perspective, a purification protocol (Scheme 3) has been developed with the objective of recovering those unreacted products the developed protocol involves the recovery of triethylamine excess through decantation and the extraction of unreacted **R0Cl** for future use in a subsequent reaction run.

Once the reaction conditions and the purification protocol were well established, the synthesis of 6 $[N_20R]Cl$-based ILs with different R substituents in the ether moiety was addressed by using different alcohols for the synthesis of the **R0Cl**. As can be seen in Fig. 3, the alkyl chains were methyl (R = 1), ethyl (2), propyl (3), isopropyl (3i), butyl (4), and isobutyl (4i). Names, purities, isolated yields, and full NMR and HRMS characterization of the ILs are available at the SI.

Fig. 3 shows decreasing $[N_20R]Cl$ isolated yields when increasing chain length and branching. This is probably due to

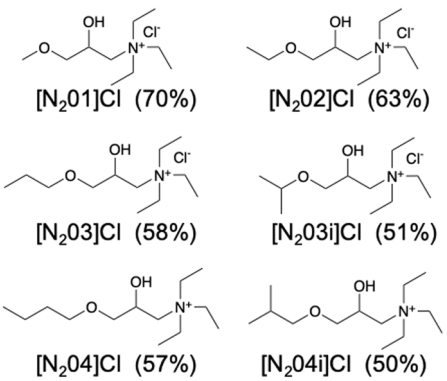

Fig. 3 Structure, code and isolated yield for the ionic liquids with chlorine as the anion prepared in this work.

steric hindrance which hinders the substitution of chlorine by triethylamine. Besides, purities of the synthesized ILs vary between 93% and 99% (Table S-1) due to the different formation of **0RCl** for the different R chains used. Consequently, a mixture of two isomeric ionic liquids, $[N_20R]Cl$ and $[N_2R0]Cl$, will be obtained in the ratio range from 1/0.01 to 1/0.07. Since these isomers have almost indistinguishable properties, they will not be separated for solvent use. Interestingly, no significant amounts of inorganic salts were quantified by ICP-AES, proving the efficacy of the purification protocol.

2.3 ILs anion exchange

After synthesizing these glycerol-derived ILs with different alkyl chains, and in order to extend the range of physicochemical properties, the synthesis of secondary families of ILs displaying different anions than chloride was envisaged. The chloride-derived ILs were subjected to anion exchange reactions for the substitution of chlorine by two inorganic anions (triflate and bistriflimide) and two organic anions (formate and lactate). As shown in Scheme 4, two different reaction protocols have been carried out. Triflates, lactates and formates have been synthesized by two consecutive reactions, first exchanging the chloride by the hydroxide and then replacing the hydroxide with the corresponding acid. The bistriflimide-based ILs, however, are synthesized directly from the chloride derivative by treatment with lithium bis(trifluoromethanesulfonyl)imide (Scheme 4).

Following this procedure, a selection of 12 new glycerol-derived ionic liquids with triflate, bistriflimide, lactate and formate anions have been prepared for the first time. These ILs bear methyl, butyl and isobutyl chains, in order to analyse the influence of the modification of the physicochemical properties with the length of the R alkyl chain. Their structures and isolated yields are shown in Fig. 4. The purification of the ionic liquids synthesized by anion exchange reactions, consisting on the precipitation of the formed salts by solvent washing and subsequent filtration, is detailed in the experimental part. These ionic liquids showed isolated yields of 60% to 83% (with respect to the chloride IL) along with purities between 94% and 97%. Note that these purity values below 100% refer mainly to the presence of residual water, and not to the presence of salts or organic by-products.

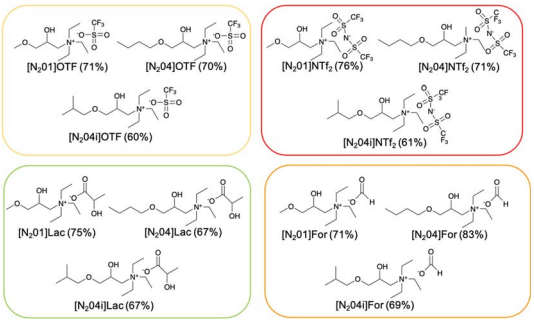

Fig. 4 Structures and isolated yields of glycerol-derived ionic liquids synthesized by ion-exchange reactions from chlorides.

In order to evaluate the sustainability of the ILs synthesis, a green metrics analysis has been carried out for the synthesis of the IL $[N_201]Cl$ starting from epichlorohydrin and methanol. For the green metrics calculations it has been considered that the heterogeneous acid catalyst K10–H^+, used in the first reaction step, can be recovered up to five times without any loss of activity, as it has been experimentally observed.

Then two scenarios have been considered (Table 3): the first one, more favourable, in which the excess of methanol in the first reaction step and the excess of the Et_3N in the second step are considered as reaction solvents and recovered for a next run, and a second scenario, in which both chemicals are considered as reagents in excess. The considered overall yield of the process is 60%. Definitions and detailed calculation of green metrics are gathered in the SI (Fig. S37 and S38).

As it can be seen, the process is theoretically well designed as the AE is 1. The use of excess of methanol in the **10Cl** synthesis and of Et_3N in $[N_201]Cl$ burdens the green metrics value, but as it has been described in the synthetic process, it is possible to recover these reagents for next runs, thus ensuring the sustainability of the process. Finally, the workup of the second reaction and the purification process of the ionic liquid greatly influences RME and MPR parameters.

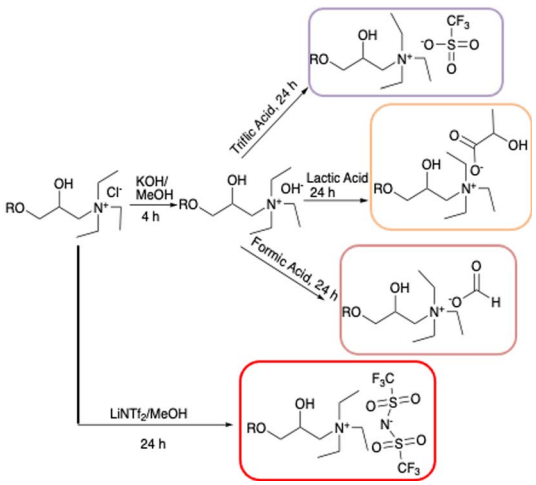

Scheme 4 Anion exchange reactions from chloride-derived ILs.

2.4 Properties of the glycerol-derived ionic liquids

All developed $[N_20R]^+$-based salts, with the single exception of $[N_204i]OTf$, can be considered as ionic liquids since they are

Table 3 Green metrics analysis for the synthesis of $[N_201]Cl$[a]

Metric	Scenario 1	Scenario 2
Atom economy (AE)	1.0	1.0
E factor	1.133	5.464
RME	0.469	0.155
MPR	0.546	0.432
Stoichiometric factor (SF)	1	1.6

[a] Scenario 1: recovery of the excess of methanol and Et_3N considered. Scenario 2: methanol and Et_3N considered exclusively as reagents and not recovered.

stable liquids at room temperature. In spite of this, a melting temperature of 328.35 K was found in the case of [$N_2$04i]OTf, so it is still an IL according to the classical definition (liquid under 373.15 K). As it is usual in bio-based ILs,[25,37,38] no liquid-crystal transitions have been observed, but the formation of different glass phases. In particular, characteristic vitreous transitions have been determined for numerous ILs, especially the ones containing chloride and lactate as anions. The temperatures for the vitreous transitions, are in a range between 241.35 K and 228.78 K (see SI). These transition temperatures seem to decrease with the length and linearity of the R alkyl chains present in the ILs.

Therefore, the working range for the developed ILs would be above room temperature (298 K), and over 243 K in most of the cases. Besides the thermal stability of the glycerol-derived ILs has been evaluated by TGA analysis (Fig. 5).

Depending on the IL anion, several groups of ILs with different stability with temperature can be observed. In general, the thermal stability trend follows the order [$N_2$0R]NTf_2 > [$N_2$0R]OTf ≫ [$N_2$0R]Cl > [$N_2$0R]Lac > [$N_2$0R]For. The maximum decomposition temperatures are, respectively for each of those families, 671.95, 637.08, 502.15, 502.35, and 490.15 K, being the most stable ILs those containing fluorinated anions. These decomposition values and trend are comparable to those of common ILs such as [BMIm]NTf_2 (726.15 K) > [BMIm]OTf (627.15 K) > [BMIm]Cl (558.15 K) and [BMIm]Ac (514.15 K).[39] As usual, the decomposition temperatures decreases slightly with the R chain length (*ca.* 2% from R = 1 to 4), due to the increase in the amount of breaking points in the IL structure.

The most relevant physical-chemical properties as solvents of the [$N_2$0R]X ILs were measured at a temperature range of 298.15–343.15(358.15) K, and the resulting experimental data were fitted to model equations. The property-temperature model parameters, gathered in the SI for the 17 glycerol-based ILs, allow to fine estimate their properties values within the whole temperature range studied.

2.4.1 Density. Density (ρ) is an essential property for the use of solvents in chemical, engineering and biological applications. Fig. 6 shows the evolution of the density values with the temperature for two selections of glycerol-derived ILs, one modifying the IL anion and the other the R-chain in the IL cation. As it is usual in solvents, ILs densities decrease with a temperature increase in all the cases. This is due to the thermal expansion of the ions contained in the IL.[40]

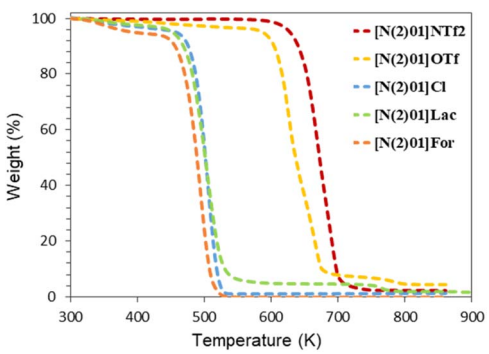

Fig. 5 TGA curves for a selection of glycerol-derived [$N_2$0R]X ILs.

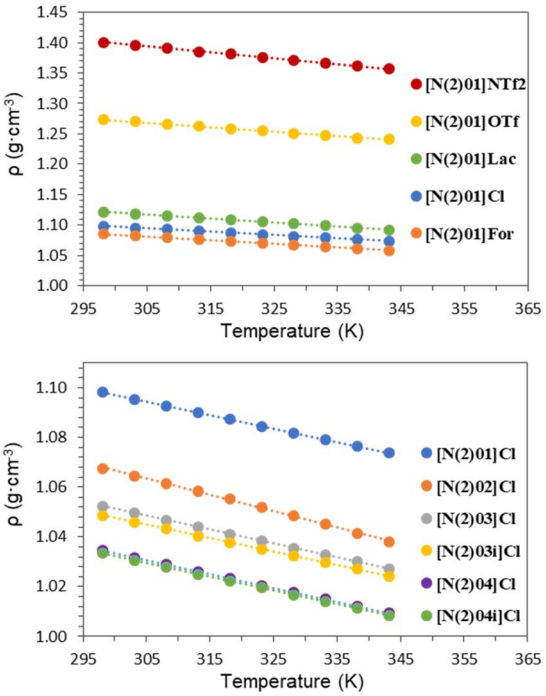

Fig. 6 Densities of glycerol-derived [$N_2$0R]X ILs.

The experimental density data were fitted to the linear eqn (1) with r^2 = 0.999–1.0000 (details in Table S-42).

$$\rho = a \cdot T + b \quad (1)$$

where ρ is the density in g cm^{-3}, T is the temperature in Kelvin, and a and b are solvent specific constants.

The influence of the IL components nature on densities can be glimpsed in Fig. 6. It can be seen that the anion has a much greater effect on the density than the cationic nature. Regarding the anion, the density trend followed the order [$N_2$0R]NTf_2 ≫ [$N_2$0R]OTf ≫ [$N_2$0R]Lac > [$N_2$0R]Cl > [$N_2$0R]For. For the case of R = 1 (methyl alkyl chain), the density values at 298.15 K are 1.40, 1.27, 1.12, 1.10, and 1.08 g cm^{-3}, respectively, showing a significant variability within this portfolio of bio-based ILs. Regarding the cation nature, the experimental density order was [$N_2$01]Cl > [$N_2$02]Cl > [$N_2$03]Cl > [$N_2$03i]Cl > [$N_2$04]Cl > [$N_2$04i]Cl. As the R-chain length and ramification increase, IL density decreases due to an increase of the volume occupied by the cations within the IL. Note that the effect of length is more significant than that of branching, as expected in organic molecules.[40] In any case, for the family of [$N_2$0R]Cl ILs, the density variation with R-chain ranges between 1.10 and 1.03 g cm^{-3} at ambient temperature.

It is interesting to compare these values with the densities displayed by other ILs, DES and typical solvents from the literature. As expected, density of glycerol-derived ILs (1.03–1.40 g cm^{-3} at 298.15 K) is higher than that of conventional organic solvents (~0.75–1.00 g cm^{-3}), but similar to those of

traditional ILs (~1.21–1.45 g cm^{-3}), cholinium and amino acid-derived ILs (1.03–1.19 g cm^{-3}), ChCl-based DES (~1.10–1.30 g cm^{-3}) and glycerol itself (1.26 g cm^{-3}).[38,41–43]

2.4.2 Molar volume. Molar volume (V_m) is a property directly related to the free volume in a liquid, which strongly influences other properties such as viscosity. The molar volume, defined as the volume in cm^3 filled by 1 mol, was calculated following the semi-empirical eqn (2), with M as the formula mass in g mol^{-1} (Tables S-7 to S-9) and ρ as the density in g cm^{-3}.

$$V_m = M/\rho \quad (2)$$

Note that the IL molar volume contains the molar masses of both the anion and the cation. Therefore, it is really dependent on the anion mass (which is very different for bistriflimide −279.92 g mol^{-1}—and for chloride −35.45 g mol^{-1}—or the organic anions—down to 45 g mol^{-1}—) and, to a lesser extent, of the R alkyl chain. Conversely, branching in the R-chain of the cation had little effect on molar volumes (Fig. 7).

Molar volume is divided by the density, thus it increases as temperature does. This inverse dependence of molar volume with temperature can be clearly seen in Fig. 7. The experimental V_m data was fitted to the linear eqn (3) with $r^2 = 0.998–1.0000$ (see fitting constants in Table S-43).

$$V_m = a \cdot T + b \quad (3)$$

where V_m is the molar volume in cm^3 mol^{-1}, T is the temperature in Kelvin, and a and b are solvent specific constants.

So, molar volume varies, respectively at 298.15 K, from 335–400 cm^3 mol^{-1} for the $[N_20R]NTf_2$ ILs, to 266–320 cm^3 mol^{-1} for $[N_20R]OTf$ ILs, to 248–307 cm^3 mol^{-1} for $[N_20R]Lac$ ILs, to 216–306 cm^3 mol^{-1} for $[N_20R]For$ ILs, and, finally, to 205–258 cm^3 mol^{-1} for $[N_20R]Cl$ ILs. This means a large range of molar volumes, beyond the values for former glycerol (73.03 cm^3 mol^{-1} at 298.15 K) and other conventional solvents.[40]

2.4.3 Viscosity. Viscosity (η) has traditionally been one of main limitations in the use and application of ionic solvents. For this reason, its determination is essential. Fig. 8 shows the shear viscosities for the glycerol-derived ILs measured at a shear velocity of 10 s^{-1}. Four effects have been studied notably affecting the ILs viscosity, the temperature (Fig. 8), the anion nature (Fig. 8a), the cation R-chain (Fig. 8b), and the IL water content (Fig. 8c). In general, viscosity is a highly temperature-dependent property, due to the exponential increase in the ionic mobility when increasing the temperature. As a result, the viscosity of the $[N_20R]X$ ILs dramatically falls when working at higher temperatures. For instance, viscosity of one of the most viscous studied ILs, $[N_201]Cl$, decreases from 81.035 to 9.096 Pa s after increasing the temperature only 20° from 298.15 K to 318.15 K.

The experimental viscosity data were successfully fitted to the Arrhenius-type eqn (4) (fitting constants in Table S-44).

$$\ln(\eta) = (E_\eta/RT) + b \quad (4)$$

where η is the viscosity in Pa s, T is the temperature in Kelvin, R is the gas constant (8.314 J K^{-1} mol^{-1}), E_η is the energy for viscous flow in kJ mol^{-1} and b is an unitless constant. The effect

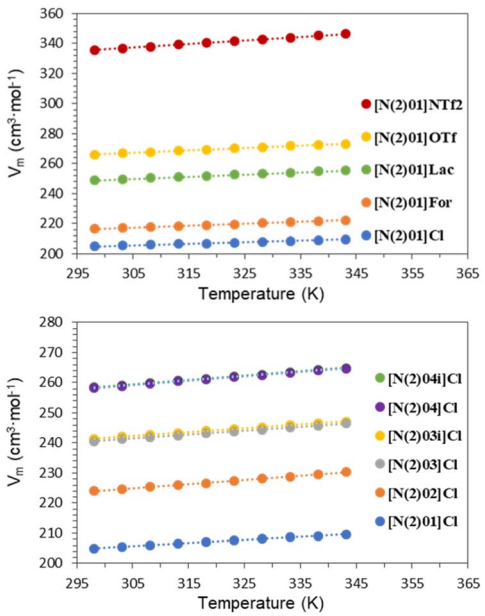

Fig. 7 Molar volumes of glycerol-derived $[N_20R]X$ ILs.

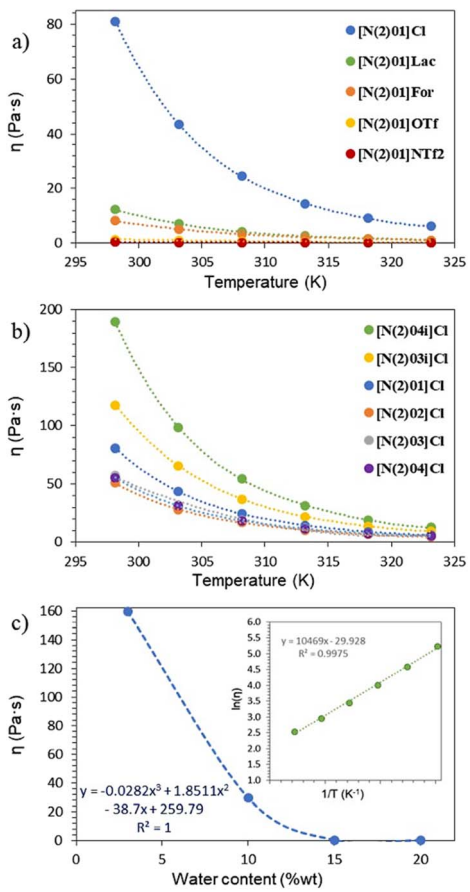

Fig. 8 Dynamic viscosities of glycerol-derived $[N_20R]X$ ILs for different (a) anions, (b) R-chains, and (c) water content in $[N_201]Cl$.

of the IL anion is really significant. The high viscosity in [N_20R]Cl ILs (50–189 Pa s) seems to be a limitation for its use at room temperature. Nevertheless, it is possible to find in the literature some ionic solvents with a similar viscosity, such as the DES based on metallic salts (*e.g.* ChCl-$ZnCl_2$ or $ZnCl_2$-EG) or the ILs based on cholinium (1–6290 Pa s) and carbohydrates (5–1476 Pa s).[25,37] When changing from [N_201]Cl to [N_201]Lac and [N_201]For, viscosity is reduced 8 times at 298.15 K. [N_201]Cl presents a lesser molar volume than the other ILs, thus its much higher viscosity must be due to its stronger intermolecular interactions. Viscosities of [N_20R]X ILs bearing organic anions (2–12 Pa s at 298.15 K) are similar to the ones of certain conventional ILs displaying large cations.[44] Finally, [N_20R]OTf and [N_20R]NTf_2 are the less viscous studied ILs, with values of around 1 and 0.3 Pa s at 298.15 K, respectively. These viscosities are very similar to traditional imidazolium-based ILs such as [BMIm]Cl, bio-based cholinium ILs, as well as to common DES such as reline (0.75 Pa s at 298.15 K) or maline (1.12 Pa s).[43] Looking deeper into the interactions affecting the viscosity, it is interesting to compare the viscosities for glycerol (1.2 Pa s at 298.15 K) and the [N_20R]Cl ILs. Despite glycerol presents a strong hydrogen bond network that usually reduces the mobility, the significant higher viscosity of the glycerol-derived ILs is caused by the introduction of ionic interactions, which hinder the diffusion through the liquid. All the aforementioned viscosity trends are also identified in the energies for activation of viscous flow (E_η, Table S-44): 75–87 kJ mol^{-1} for [N_20R]Cl, 50–75 kJ mol^{-1} for [N_20R]Lac/For, and 43–55 kJ mol^{-1} for [N_20R]OTf/NTf_2. In any case, these values are similar to many ILs and DES.[45]

Interestingly, and oppositely to other ILs and DES such as ChCl–R00,[40] the viscosity of the glycerol-based ILs does not seem to increase with the R-chain length. Also, a slight odd-even effect is observed, increasing the viscosity for the odd R-chains. This behaviour, which is contrary to the expected trend related to the formation of interactions in longer R-chains, could be more likely explained by the presence of residual or structural water in the ILs. This water content varies according to the hydrophobicity of the corresponding IL and it would be responsible for modifying the expected viscosity trends.

In order to understand the magnitude of the water effect on the studied ILs viscosity, the viscosity of [N_201]Cl at 293.15 K with different water contents was evaluated. As can be seen in Fig. 8c, a quasi-exponential viscosity decrease is observed. So that, increasing the water content from 3 wt% to 10 wt%, 82% viscosity reduction is achieved (99.7% reduction for +15 wt%). This is very important point as it opens the door to the use of viscous [N_20R]Cl ILs for industrial applications, even controlling the exact viscosity of the fluid with the water content.

Finally, the presence of a ramification in the R-chain leads to a notable increase in the IL viscosity. This phenomenon, related to both intermolecular interactions and the diffusion through different sizes of holes created in the ionic medium, has been reported in the literature for organic solvents, ILs and DES.[40,46]

2.4.4 Refractivity and polarizability. Refractive index (n_D) is a relevant property for a solvent, as it can provide information about its polarizability and purity. Fig. 9 shows the dependence of the refractive index with temperature for the two groups of glycerol-derived ILs. In the case of studying the anion effect, the refractive index trend followed the sequence [N_20R]Cl > [N_20R]For > [N_20R]Lac > [N_20R]OTf > [N_20R]NTf_2. For the case of R = 1, it is interesting to see the significant variation, 1.5057, 1.4858, 1.4768, 1.4372, and 1.4292, respectively at 298.15 K. This trend can also be found for imidazolium ILs displaying the same anions.[47]

Regarding the cation R-chain, the observed refraction order was [N_201]Cl > [N_202]Cl > [N_203]Cl > [N_203i]Cl > [N_204i]Cl > [N_204]Cl. This variation in the refractive index can be explained by the lower density of the IL when substituted by longer R alkyl chains (that decreases the n_D by an increase in the light propagation speed).[40] This trend was observed for all the families with the exception of [N_20R]NTf_2. This particular opposite trend for the case of [N_20R]NTf_2 ILs probably appears because the above-mentioned decrease of n_D with the lower density, when increasing the R-chain length, is an effect that is counteracted by the higher polarizability of a longer cation.[40]

These experimental refractive indices are characteristic for each glycerol-derived IL, but they are close to those of other

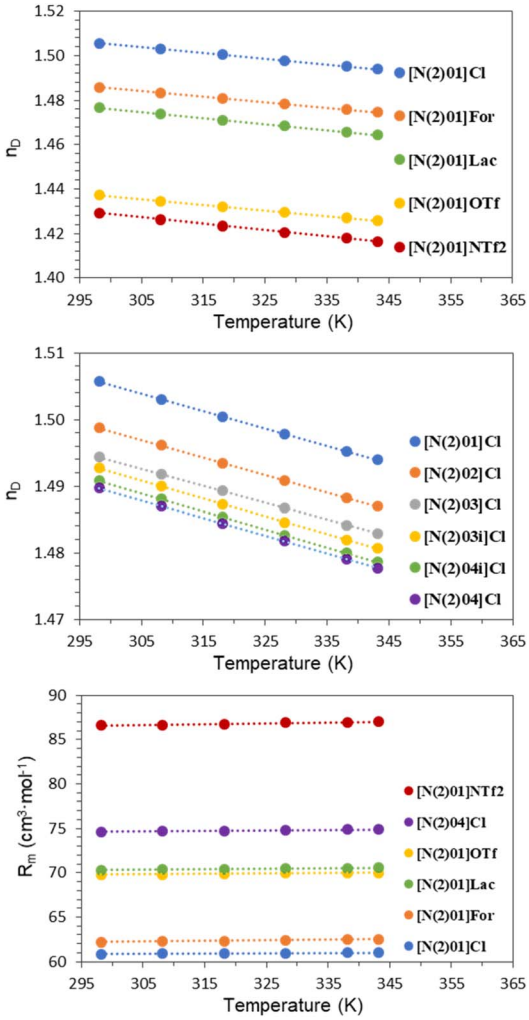

Fig. 9 Refractive indices and molar refractivities of [N_20R]X ILs.

solvents, including organic solvents (~1.32–1.50) and glycerol (1.47),[40] classic ILs, and bio-ILs based on amino acidic cations (1.48–1.54).[38,42]

Molar refractivity (R_m) is a related property that minimize the strong dependence of n_D with the temperature in order to show the electronic polarizability effect. This electronic polarizability shows the capacity of the orbitals to be deformed by an electric field, and thus can provide information about solvation effects. With this aim, molar refractivities were calculated using the Lorentz equation (eqn (5)).

$$R_m = \frac{{n_D}^2 - 1}{{n_D}^2 + 2} \cdot V_m \quad (5)$$

where R_m is the molar refractivity in $cm^3\ mol^{-1}$, n_D is the refractive index, and V_m is the molar volume in $cm^3\ mol^{-1}$.

As observed in Fig. 9, the R_m trend is always the opposite to the one observed for n_D values because of the single dependence on polarizability. As a consequence of this, larger and more nonsymmetric IL cations and anions significantly increases the molar refractivity, thus the IL polarizability. Some examples are $(NTf_2) > (Lac) > (For) > (Cl)$ for the anion and $[N_201]Cl \ll [N_204]Cl$ for the cation.

The experimental n_D and R_m data were fitted to the linear eqn (6) and (7) with $r^2 = 0.9998–1.0000$ and 0.97–0.9990 respectively (see fitting constants in Tables S-45 and S-46).

$$n_D = a \cdot T + b \quad (6)$$

$$R_m = a \cdot T + b \quad (7)$$

where n_D is the refractive index, R_m is in $cm^3\ mol^{-1}$, T is the temperature in Kelvin, and a and b are refractivity constants.

2.4.5 Miscibility with organic solvents. $[N_20R]X$-based ILs are highly-polar ionic solvents whose polarity is supposed to be modulated by the anion and, to a lesser extent, by the R-chain length of the cation. In general, these glycerol-derived ILs are miscible with water and conventional organic solvents including dichloromethane (DCM), dimethylsulfoxide (DMSO), and short-chained alcohols such as methanol, but immiscible with hydrocarbons such as hexane. Table S-41 gathers the miscibility of $[N_20R]X$ in these traditional organic solvents. It can be seen that for Cl, OTf, For and Lac derivatives, total miscibility can be seen with the polar solvents but no miscibility with hexane is observed. In the case of $[N_20R]NTf_2$, these ILs are both immiscible with water, due to its more hydrophobic anion, and hexane, due to its ionic nature. This generates a polarity difference that can be exploited for extraction or solubilization processes.

In order to estimate the ILs bioaccumulation and thus the possible toxicity impact, the log P of representative ILs containing the same $[N_204]^+$ cation and different X^- anions was experimentally determined and compared to the ones of ammonium ionic liquids described in the literature (Fig. 10).[48,49] Butyl derivatives were selected as representative of the most hydrophobic ILs, being aware that the modification of the alkyl chain to shorter substituents in the cation would decrease the log P value and thus the possible toxicity.

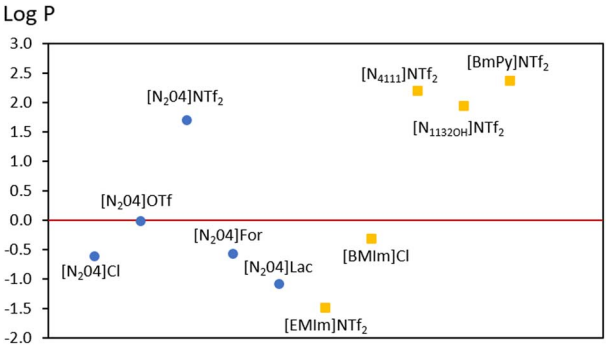

Fig. 10 Comparison of log P values of $[N_204]X$ ILs (this work) with some values examples from the literature.[48,49]

As it can be seen, all our ILs showed log $P < 0$ being then more prompt to be water soluble, except for the NTf_2 derivatives. In that case, the log P value is similar to other ammonium derivatives described in the literature. Therefore, most of the ILs described herein can be considered as very low to low bioaccumulative compounds, notably minimizing their environmental and human risks.

2.4.6 Green solvent features. These new ILs derived from glycerol are renewable solvents, since they can be obtained from renewable feedstock through sustainable synthetic methodologies. On the other hand, toxicity of these bio-based ILs has not yet been experimentally evaluated. However, we recently reported the almost negligible ecotoxicity of the chemically analogous $[N_200]Cl$ salt,[15] which prompt us to reasonably anticipate a low toxicity, especially for ILs with Cl and organic anions in their composition, as has also been indicated by the experimental log P values.

It is very interesting to represent properties maps to locate the developed ILs (Fig. 11 in blue) with respect to other common ILs and DES (in green) and even molecular solvents (in red and gold). According the features of these ILs, we decided to generate the maps of density *vs.* viscosity and molar refractivity. In the first map it is possible to see that glycerol-based ILs have counterparts with similar rheological characteristics than a long series of ionic solvents from the literature, with the exception of $[N_20R]Cl$. More interestingly, the second map shows that the new ILs occupy a space for highly polarizable solvents where no traditional solvent is situated, thus revealing new solvents with unique properties for solubilization purposes.

2.5 Application examples

As stated in the introduction, two applications have been envisaged for the new ionic liquids: the solubilisation of products of interest, namely hydroxycinnamic acids, and the design of recoverable catalytic systems based on palladium nanoparticles (Pd NPs). For it, the performance of the selection of new bio-based ILs gathered in Fig. 12 will be compared to that of other classical ILs and DES reported in the literature.

2.5.1 Hydroxycinnamic acids solubility study. Insoluble phenolic compounds are integral components of the plant cell

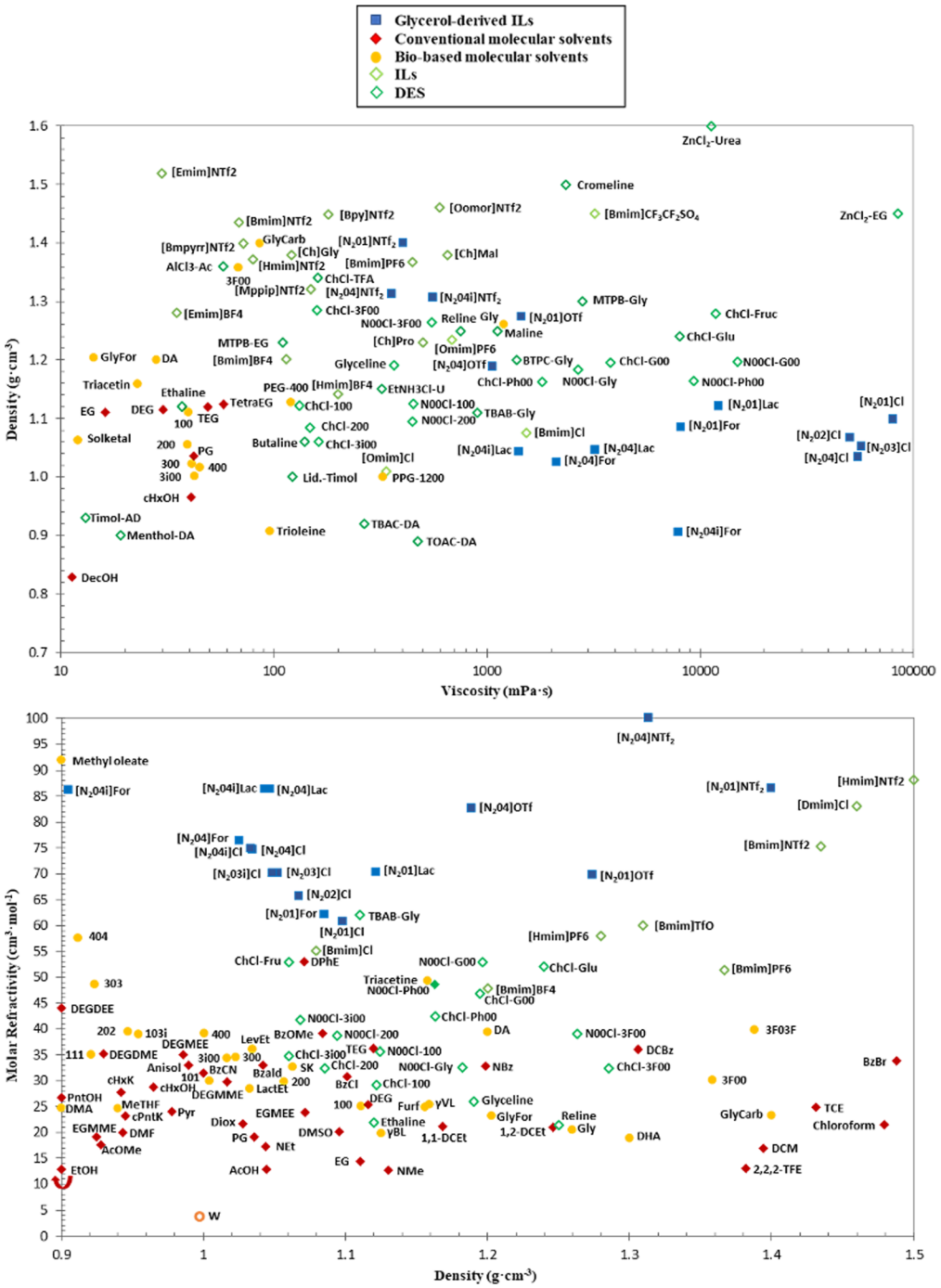

Fig. 11 Properties maps of developed glycerol-derived ILs [N_20R]X (in blue) with respect to common ILs and DES (in green), traditional molecular solvents (in red) and bio-based molecular solvents (in gold), representing density *vs.* viscosity and molar refractivity *vs.* density.

membranes. Many of them, based on hydroxycinnamic acids such as ferulic, coumaric, and caffeic acids, present interesting antioxidant,[50–52] and antimutagenic properties.[53] This makes their solubilisation of interest for extraction processes and for the preparation of formulations.

In this study, both the influence of the nature of the IL R substituent and anion has been considered. As a consequence of this, four ILs were evaluated as solubilisation solvents, namely [N_201]Cl, [N_204]Cl, [N_201]OTf and [N_204]OTf. It should be noted that all the tested solvents had a 10% water content as determined by TGA. The presence of water aided the solubility process just by significantly reducing the viscosity of the media, as it is known that water is a very poor solvent for these acids.

As it can be seen in Fig. 13, coumaric acid is the most soluble hydroxycinnamic acid, followed by ferulic and caffeic acids. The influence of the cationic R-chain (methyl or butyl) is almost negligible in all the cases, but this is not the case for the influence of the anion. The use of [N_20R]Cl strongly favoured

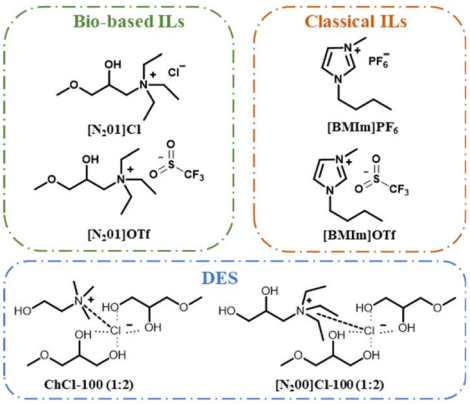

Fig. 12 Structures of the ionic solvents used in the example applications.

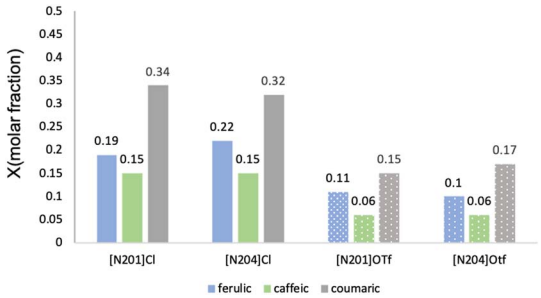

Fig. 13 Solubilities (X) of ferulic, caffeic and coumaric acids in several glycerol-derived ILs.

the solubility of the three hydroxycinnamic acids compared with the use of $[N_201]$OTf. This demonstrates the significant impact of the anion's coordinating capacity in forming hydrogen bonds with the OH groups of solutes, which facilitates their solubilisation even despite the much higher viscosity of $[N_20R]$Cl ILs.

This preliminary study highlights the importance of having a portfolio of solvents similar in structure for a better understanding and optimization of the solubilization process. The obtained solubilities exceed, in some cases by far, those previously described in the literature (Table 4). As it can be seen, for ferulic acid, the ILs $[N_201]$Cl and $[N_204]$Cl provided much better results than some conventional solvents such as ethanol, propylene glycol or PEG-400 reported by Shakeel *et al.*[54] In the case of caffeic and coumaric acids, the solubilities described in this work are much higher than the ones described by Wang[55] and Alevizou[56] using ethanol, *n*-pentanol or a conventional IL such as [BMIm]OTf.

2.5.2 Recoverable catalytic system design study. As a second application, the preparation of recoverable catalytic systems based on Pd NPs was envisaged. Two ionic liquids, $[N_201]$Cl and $[N_201]$OTf, were chosen in order to compare the results with those of previous catalytic systems immobilized within a glycerol monoether (3-methoxypropan-1,2-diol, 100) and DES formed with this ether and two ammonium salts (ChCl and N00Cl) (Fig. 12).[57]

Table 4 Solubility values of ferulic, caffeic and coumaric acids in different solvents

Solute	Solvent	Molar fraction X	Ref.
Ferulic acid	EtOH	0.0241	54
Ferulic acid	Propylene glycol	0.0263	54
Ferulic acid	PEG-400	0.154	54
Ferulic acid	$[N_201]$Cl	0.194	This work
Ferulic acid	$[N_204]$Cl	0.224	This work
Caffeic acid	EtOH	0.0166	55
Caffeic acid	*n*-Pentanol	0.0184	56
Caffeic acid	[BMIm]OTf	0.0204	56
Caffeic acid	$[N_201]$Cl	0.151	This work
Caffeic acid	$[N_204]$Cl	0.155	This work
Coumaric acid	EtOH	0.0456	55
Coumaric acid	*n*-Pentanol	0.0744	56
Coumaric acid	[BMIm]OTf	0.1054	56
Coumaric acid	$[N_201]$Cl	0.342	This work
Coumaric acid	$[N_204]$Cl	0.324	This work

The Heck–Mizoroki coupling between iodobenzene and *n*-butyl acrylate was chosen as a benchmark reaction (Scheme 5) to study catalytic activity and selectivity to butyl cinnamate, a compound very appreciated in dermatology and cosmetics.

Once the 0.3 mol% Pd NPs suspension was obtained in ethanol, the nanoparticles were immobilized in the selected glycerol-derived solvents during the removal of the ethanol under vacuum. The two Pd NPs/$[N_201]$X catalytic systems were characterized by transmission electron microscopy (TEM, Fig. 14). In all cases, small size nanoparticles are obtained, with average diameters of 2.6 ± 0.8 nm for the case of $[N_201]$OTf (almost identical to that of fresh Pd NPs in ethanol) and 3.2 ± 0.6 nm for $[N_201]$Cl. Interestingly, the combination of the higher viscosity and anion coordinating capacity, in the case of $[N_201]$Cl with respect to $[N_201]$OTf, seems to favour a more homogeneous dispersion of the nanoparticles.

Both catalytic systems Pd NPs/$[N_201]$Cl and Pd NPs/$[N_201]$OTf were tested in the benchmark reaction and fully recovered upon 5 consecutive runs providing quantitative yields and cinnamate selectivities, with an accumulated TON of 1500.

Comparing these results with the previously reported using Pd NPs immobilised on the glycerol monoether and the two mentioned DES, it can be observed that the Pd NPs immobilized in the new glycerol ILs had a significant better performance (Table 5). Surprisingly, the NPs distribution differences between the two studied $[N_201]$X ILs did not seem to affect the resulting catalytic activity. Furthermore, in the case of using these ILs, no leaching of solvent into the extraction media was observed, whereas in the case of using DES or glycerol monoether, an

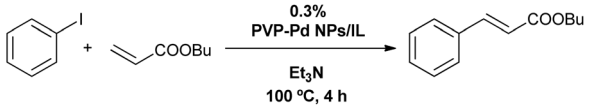

Scheme 5 Heck–Mizoroki reaction of iodobenzene and *n*-butyl acrylate catalyzed by Pd NPs immobilized in glycerol-derived ILs.

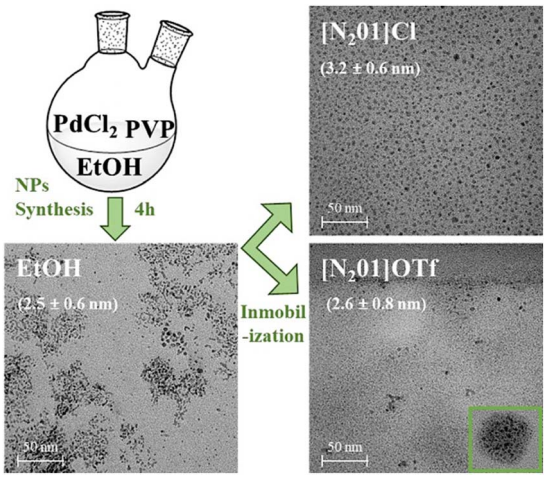

Fig. 14 TEM Images of Pd NPs in ethanol, [$N_2$01]Cl and [$N_2$01]OTf.

Table 5 Average yield and accumulated TON (for 5 cycles) Heck–Mizoroki coupling reaction of iodobenzene and *n*-butyl acrylate catalyzed by Pd NPs/glycerol-derived solvent

Solvent	Average yield (%)	Accumulated TON	Ref.
100 monoether	92	1366	57
DES (ChCl-100)	94	1399	57
DES (N00Cl-100)	96	1420	57
[BMIm]PF_6 IL	91	1354	57
[$N_2$01]Cl IL	100	1500	This work
[$N_2$01]OTf IL	100	1500	This work

amount of about 3% of the glycerol ether was extracted along with the reaction product.

It is also noteworthy the stability of the solvent in the basic reaction media.

The unique properties of these bio-based ionic liquids, particularly their tunable hydrogen-bonding capacity (evident in Cl^-/Lac^- variants) and thermal stability, position them as promising candidates for biomass processing, where they could serve as sustainable solvents for lignocellulose dissolution, and potentially outperforming conventional imidazolium-based ILs in biorefinery applications. Additionally, the lower viscosity and robust thermal stability of [$N_2$0R]NTf_2/OTf systems suggest their suitability for electrochemical devices, such as high-performance electrolytes in batteries or supercapacitors, combining renewable sourcing with the wide electrochemical windows required for energy storage. Beyond these fields, their modular design might enable innovative uses in CO_2 capture (leveraging formate/lactate anions for chemisorption) or as stabilizing media for biocatalysis, where their biocompatibility could enhance enzyme activity in non-aqueous environments.

3 Experimental

Ethanol, epichlorohydrin, 2-methylpropan-1-ol, formic acid, *n*-butyl acrylate, PVP, *n*-decane, montmorillonite K10, $Pd(AcO)_2$, caffeic acid (98% purity; CAS No. 331-39-5), coumaric acid (98% purity; CAS No. 501-98-4) and ferulic acid (99% purity; CAS No. 537-98-4) were purchased from Sigma-Aldrich. Hydrochloric acid, triethylamine, potassium hydroxide, 1-propanol, 2-propanol, 1-butanol and DL-lactic acid were purchased from Fischer Scientific. Alkyl glycidyl ethers were acquired from TCI, triflic acid and lithium bis(trifluoromethanesulfonyl)imide from Fluorochem, methanol, iodobenzene, and the acetonitrile required for HPLC measurements were purchase from Alfa Aesar, and Milli-Q® water was used for these measurements.

All the synthesized ILs were characterized and their purity was determined by ^{1}H NMR and HRMS.

3.1 Synthesis of glycerol-derived ionic liquids

3.1.1 Synthesis from alkyl glycidyl ether. The appropriate amount of triethylamine (5 mmol) was placed into a round-bottomed flask. Then, the corresponding glycidyl ether (5 mmol) and hydrochloric acid (5 mmol) were added dropwise to the reaction. It is important to control the addition rate of both reagents, the best results being obtained when the addition rate of HCl was 1/6 of that of glycidyl ether. The reaction was stirred at 80 °C for 48 h under argon atmosphere. Afterwards, the triethylamine excess was recovered and the reaction mixture was diluted with water (10 mL) and extracted with diethyl ether (3 × 10 mL). Triethylammonium chloride salt was removed by treatment with K_2CO_3 (stoichiometric amount with respect to the salt), heating at 100 °C for 24 h. After this time, the mixture was cooled down, filtered off and dried.

3.1.2 Synthesis from epichlorohydrin

*3.1.2.1 Synthesis of 1-chloro-3-alkoxypropan-2-ol (**R0Cl**).* The corresponding amount of alcohol (7.5 : 1 mol with respect to epichlorohydrin) and the heterogeneous catalyst (montmorillonite K10, 10% mol with respect to epichlorohydrin) were placed in a 2 L reactor and heated at 65 °C. Then, epichlorohydrin (1.6 mol) was added dropwise. The reaction was monitored by GC. Once the epichlorohydrin was consumed, the product was removed from the reactor, the catalyst was filtered out and the alcohol excess was removed by vacuum distillation.

3.1.2.2 Synthesis of N,N,N-triethyl-2-hydroxy-3-alkoxypropan-1-ammonium [$N_2$0R]Cl. The appropriate amount of triethylamine (0.3 mol) was placed into a round-bottomed flask. Then, the corresponding 1-chloro-3-alkoxypropan-2-ol (0.3 mol) was added dropwise. The reaction was stirred and heated at 100 °C for 7 days under argon atmosphere. Throughout this time, 50% triethylamine excess (0.15 mol) was added every 48 h. The reaction product was analysed prior to its purification. Then, the triethylamine excess was recovered and the reaction mixture was diluted with water (50 mL) and extracted with diethyl ether (3 × 50 mL) to remove the unreacted **R0Cl**. Triethylammonium chloride salt was removed by treatment with K_2CO_3 (stoichiometric amount with respect to the salt), heating at 100 °C for 24 h. After this time, the mixture was cooled down and filtered. To remove coloured impurities, the IL was mixed with water and activated carbon and stirred for 1 h. This mixture was filtered and most of water was removed by vacuum distillation. Finally, the IL was dried by lyophilisation in

a freeze-dryer (model SCANVAC Coolsafe 110-4Pro) for 24 h and then under vacuum heating at 80 °C for 5 h.

3.1.2.3 Synthesis of ammonium bistriflimidate [N_20R]NTf_2. In a round bottom flask, the appropriate amount of the chloride-based IL (0.06 mol) was dissolved in methanol (100 mL) and the equimolecular amount of bis(trifluoromethylsulfonyl)imide lithium was added. The mixture was stirred at room temperature for 24 h under argon atmosphere. After this time, the lithium chloride was filtered off and methanol was removed under vacuum. Finally, the IL was lyophilized and dried under vacuum at 80 °C for 5 h.

3.1.2.4 Synthesis of ammonium triflates, lactates, and formates [$N_2$0R]X. In a round bottom flask, the appropriate amount of the chloride-based IL (0.06 mol) was dissolved in methanol (50 mL) and mixed with the equimolecular amount of potassium hydroxide dissolved in methanol (50 mL). The mixture was stirred at room temperature for 3 h under argon atmosphere. After this time, the formed potassium chloride was filtered off. The obtained product was mixed with the equimolecular amount of acid (triflic, lactic or formic) and kept under argon atmosphere and constant stirring for 24 h at r.t. Afterwards, methanol was removed by vacuum distillation and the remaining KCl salt was precipitated from the liquid phase by washing with ether. Then, this salt was filtered off and the washing solvent was removed by vacuum distillation. Finally, the IL was dried heating at 80 °C under vacuum for 5 h.

All the yields provided are isolated yields calculated by weighting the IL after purification.

3.2 Characterization of physicochemical properties

3.2.1 Thermal stability. Thermogravimetric analysis (TGA) was carried out to determine the ILs decomposition onset. TGA measurements were performed using a TA Instruments 2960 SDT V3.0F. Samples were measured in platinum pans under a dynamic nitrogen flow of 50 mL min^{-1}, and heated up to 600 °C with a 10 °C min^{-1} gradient.

3.2.2 Differential scanning calorimeter (DSC). DSC measurements were performed for determination of phase transitions using a DSC Q20 TA Instruments. Samples were measured in Tzero aluminium hermetic pans under a dynamic nitrogen flow of 50 mL min^{-1} and indium as the standard. Six cycles were carried out with a temperature programme consisted of a 10 °C min^{-1} gradient from −50 to 100 °C, followed by a −10 °C min^{-1} gradient from 100 to −50 °C.

3.2.3 Density. ILs density was determined using an Anton Paar DSA 5000 densimeter. Calibration of the equipment was carried out using dry air and ultrapure water (SH Calibration Service GmbH). The temperature was controlled internally with an uncertainty of ±0.01 K. The uncertainty for the density measurements was 5×10^{-3} kg m^{-3}.

3.2.4 Molar volume. ILs molar volume was calculated from the density measurements using the eqn (2).

3.2.5 Viscosity. A series of shear viscosity measurements were performed on ILs samples using a HaakeTM MarsTM 40 rheometer equipped with a cone-plane measuring geometry at varying temperature ($\dot{\gamma}$ constant of 10 s^{-1}).

3.2.6 Refractivity. The refractive index was determined using an Abbemat-HP refractometer Dr Kernchen with a sodium lamp (D wavelength at 589.3 nm). The temperature was controlled internally (with uncertainty of ±0.01 K). The uncertainty for refractive index measurements was $\pm 5 \times 10^{-5}$.

3.2.7 Miscibilities. Five organic solvents of different polarity (water, methanol, dimethylsulfoxide, dichloromethane, and *n*-hexane) were selected for the ILs solubility studies. In a 2 mL Eppendorf tube, 0.2 mL of the IL, together with 0.2 mL of the organic solvent were added. The mixture was kept under stirring at room temperature for 1 h. After this time, the mixture was kept at rest for 1 h to ensure a correct phase separation. The organic phase was then extracted, the organic solvent was evaporated, and the residue was analysed by ^{1}H NMR to determine the amount of IL remaining in the organic phase. To ensure an accurate quantification, anisole (10 μL) was added as a standard to the NMR tube.

3.2.8 Log P measurements. In a centrifuge tube, 5 mL of water and a 5 mL octanol solution containing 0.1 M of the corresponding ionic liquid were added. The mixture was stirred under sonication for 3 h and then centrifuged for 1 h at a speed of 4000 rpm to ensure complete phase separation. Water was removed under reduced pressure prior to the determination of the ionic liquid contained in the aqueous phase by ^{1}H NMR using anisole as a standard. The organic phase was heated at 100 °C under vacuum for 5 h to remove octanol, and the ionic liquid present was also analysed by ^{1}H NMR using anisole as standard. For the calculation of log P the eqn (8) was applied, where [IL] refers the concentration of the ionic liquid in each of the phases.

$$\log P_{\mathrm{oct/wat}} = \log_{10}\left(\frac{[\mathrm{IL}]_{\mathrm{oct}}}{[\mathrm{IL}]_{\mathrm{wat}}}\right) \quad (8)$$

3.3 Hydroxycinnamic acids solubility study

For solubilities determination, saturated solutions were prepared by adding 100 mg of hydroxycinnamic acid to 250 μL of the solvent. Amber vials were used in order to protect samples from light. To ensure reliability, all the experiments were performed in triplicate. The samples were magnetically stirred for 72 h at 25 °C. Preliminary experiments were performed to determine the equilibrium time, and 72 h was found to be the optimal time. After that time, the samples were microfiltered using a Teflon® microfilter (0.4 mm) and the appropriate dilutions were made in such a way that the concentration was adequate for subsequent measurement by high-performance liquid chromatography (HPLC).

HPLC analysis was performed on a Waters 2690 Separations chromatograph in reverse phase, equipped with a Waters 2996 Photodiode Array ultraviolet detector. Quantification was carried out using a C18 Phenomenex® Luna column (150 mm x 4.6 mm, 5 μm particle size). The injection volume was set to 10 μL, and the elution was performed at a flow rate of 10 mL min^{-1}. For the mobile phase, a methanol : water (40 : 60) : 0.1% TFA mixture was used for the analysis of coumaric and caffeic acids, while acetonitrile : water (30 : 70) : 0.1% TFA was used for ferulic

acid. Calibration curves were constructed using solutions of varying concentrations of the three acids under study. These solutions were prepared within the HPLC detection range (0–0.006 mg). Before injection into the HPLC, the solutions were sonicated to ensure uniform peak distribution and avoid the formation of dimers. The linearity of the calibration curves was assessed using linear regression analysis. Further details of the calibrations can be found in the SI.

3.4 Recoverable catalytic system design study

Pd NPs were synthesized in 3 h by reduction of H_2PdCl_4 (2 mM) as the palladium precursor, using ethanol (94 mL) as reductant and reflux solvent, and PVP (444.6 mg) as an organic stabilizer, as described in our previous work.[57] Then, the PVP-Pd NPs were suspended into absolute ethanol (66 mL). Finally, the same volume of glycerol-derived solvent was added and stirred for 20 min, prior to the removal of ethanol under vacuum. For the Heck–Mizoroki coupling reactions, 1 mL of PVP-Pd NPs/glycerol-derived solvent (0.3 mol% Pd) was placed into a 20 mL Schlenk flask. Then a reaction mixture formed by 0.1 mL of iodobenzene (0.9 mmol), 0.2 mL of *n*-butyl acrylate (1.4 mmol) and 0.3 mL of triethylamine (2.17 mmol) was added. The closed Schlenk flask under argon atmosphere was stirred and heated at 100 °C for 4 h. After this time, the system was cooled down and the mixture was extracted with *n*-pentane (2 × 10 mL and 2 × 5 mL) at 65 °C using vigorous stirring and 20 min periods between extractions. Finally, the catalytic system was dried under vacuum prior to a new reaction cycle. Conversions and yields were determined by gas chromatography using *n*-decane as a standard with a Hewlett Packard 7890 Series II chromatograph equipped with a column of phenyl silicone 5.5% (Zebron ZB-5HT Inferno 30 m × 0.25 mm × 0.25 μm) and helium as carrier gas, and equipped with a Flame Ionization Detector (FID). GC temperature programs and calibrations are gathered in the SI.

4 Conclusions

This work successfully presents a novel family of glycerol-derived ionic liquids ([N_20R]X) with tailored properties, bridging the gap between sustainability and performance in ionic solvents.

An easy, safe and affordable and scalable synthetic procedure has been developed starting form epichlorohydrin and yielding ILs with high purity (93–99%) and modular structures. The physicochemical properties of the new biobased ILs are tunable, since for instance viscosity, density, and thermal stability were finely adjustable *via* anion selection (NTf_2 > OTf > Cl ≈ Lac > For) and also through R alkyl chain length selection, enabling customization for specific applications.

A preliminary study of the utility of these solvents, both as solubilisation and reaction media, have demonstrated their applicability and potential, for instance surpassing conventional solvents (*e.g.*, ethanol and [BMIm]OTf) in hydroxycinnamic acids solubilisation due to strong hydrogen-bonding interactions, or acting as effective solvents in the design of recoverable catalytic systems based on Pd NPs.

Despite these promising results, glycerol-derived ionic liquids present challenges that must be addressed to fully realize their potential. Notably, the high viscosities observed for [N_20R]Cl systems (50–189 Pa s at 298 K) may limit their suitability for industrial processes requiring efficient mass transfer or rapid flow. Nevertheless, it has been proved here that viscosity of these ILs can be controlled and bypassed by applying temperature or adding water, neglecting this major limitation for classic imidazolium ILs. Furthermore, the lengthy synthesis times (up to 168 h) and the need for stoichiometric excesses of triethylamine in some routes raise concerns about economic scalability.

However, these limitations do not overshadow the core value of this work, as the tunable properties, some of them covering empty solvent spaces, their renewable origin, and superior performance in key applications (*e.g.*, hydroxycinnamic acid solubilisation and catalysis) position this IL family as a viable alternative to conventional solvents, particularly if future optimizations streamline synthesis and reduce costs. It is expected that future work should explore broader toxicity assessments and additional applications (*e.g.*, biomass processing, electrochemistry) to fully exploit the potential of glycerol-derived ILs.

Author contributions

Conceptualization: E. Pires, J. A, Mayoral and A. Leal-Duaso. Data curation A. Leal-Duaso and S. Gracia Barberán. Funding acquisition: E. Pires, A. Leal-Duaso and J. del Barrio. Investigation and methodology: S. Gracia Barberán, J. del Barrio, A. Leal-Duaso. Supervision: E. Pires. Writing original draft: E. Pires, S. Gracia Barberán, A. Leal-Duaso. Writing – review and editing: E. Pires, S. Gracia Barberán, A. Leal-Duaso, J. del Barrio and J. A. Mayoral.

Conflicts of interest

There are no conflicts to declare.

Data availability

The full data supporting this article have been included as part of the SI. See DOI: **https://doi.org/10.1039/d5su00393h**.

Acknowledgements

S. G.-B. thanks the Cátedra SAMCA de desarrollo tecnológico de Aragón for her contract. A. L.-D. acknowledges the "Programa Margarita Salas 2021–2023" (Plan Nacional de Recuperación, Transformación y Resiliencia) financed by the European Union-NextGenerationEU through the Ministerio de Universidades of Spain and the University of Zaragoza. J. d. B. acknowledges grant PID2023-147656OB-I00 funded by MICIU/AEI/10.13039/501100011033 and by FEDER, UE. Authors would like to acknowledge the Servicio General de Apoyo a la Investigación-SAI, Universidad de Zaragoza and Laboratorio de

Microscopías Avanzadas-LMA (INMA-Unizar), Servicios Científicos Técnicos of CEQMA (CSIC-Unizar), and C. Lafuente for providing densimeter and refractometer instruments. This work has been supported by the Spanish Agency of Research (AEI) (project PID2021-125762NB-I00), the Gobierno de Aragón (E37_23R group), and the European Union NextGenerationEU founds.

Notes and references

1 T. Welton, *Green Chem.*, 2011, **13**, 225.
2 G. Kaur, H. Kumar and M. Singla, *J. Mol. Liq.*, 2022, **351**, 118556.
3 S. K. Singh and A. W. Savoy, *J. Mol. Liq.*, 2020, **297**, 112038.
4 K. Kuroda, *New J. Chem.*, 2022, **46**, 20047–20052.
5 D. Zhao, Y. Liao and Z. Zhang, *Clean: Soil, Air, Water*, 2007, **35**, 42–48.
6 Himani, A. P. S. Raman, M. Babu Singh, P. Jain, P. Chaudhary, I. Bahadur, K. Lal, V. Kumar and P. Singh, *J. Mol. Liq.*, 2022, **364**, 119989.
7 S. Gracia-Barberán, A. Leal-Duaso and E. Pires, *Curr. Opin. Green Sustainable Chem.*, 2022, **35**, 100610.
8 A. Leal-Duaso, Y. Adjez and C. M. Sánchez-Sánchez, *ChemElectroChem*, 2024, **11**, e202300771.
9 E. L. Smith, A. P. Abbott and K. S. Ryder, *Chem. Rev.*, 2014, **114**, 11060–11082.
10 F. M. Perna, P. Vitale and V. Capriati, *Curr. Opin. Green Sustainable Chem.*, 2020, **21**, 27–33.
11 L. Cicco, G. Dilauro, F. M. Perna, P. Vitale and V. Capriati, *Org. Biomol. Chem.*, 2021, **19**, 2558–2577.
12 A. F. Monroy, G. A. Caicedo, J. J. Martínez and G. P. Romanelli, *Biofuels, Bioprod. Biorefin.*, 2024, **18**, 1821–1865.
13 D. Yu, D. Jiang, Z. Xue and T. Mu, *Green Chem.*, 2024, **26**, 7478–7507.
14 Y. Li, M. Sun, Y. Cao, K. Yu, Z. Fan and Y. Cao, *ChemSusChem*, 2024, **17**, e202301953.
15 M. P. Garralaga, L. Lomba, A. Leal-Duaso, S. Gracia-Barberán, E. Pires and B. Giner, *Green Chem.*, 2022, **24**, 5228–5241.
16 A. A. Quintana, A. M. Sztapka, V. d. C. Santos Ebinuma and C. Agatemor, *Angew. Chem., Int. Ed.*, 2022, **61**, e202205609.
17 J. Hulsbosch, D. E. De Vos, K. Binnemans and R. Ameloot, *ACS Sustainable Chem. Eng.*, 2016, **4**, 2917–2931.
18 J. M. Gomes, S. S. Silva and R. L. Reis, *Chem. Soc. Rev.*, 2019, **48**, 4317–4335.
19 J. M. Costa, T. Forster-Carneiro and J. P. Hallett, *Green Chem.*, 2024, **26**, 705–719.
20 Y. Zheng, Y. Dai, Y. Hong, S. Dai, C. Wang, Y. Cai and K. Wang, *J. Mol. Liq.*, 2024, **404**, 124972.
21 S. Kirchhecker and D. Esposito, *Curr. Opin. Green Sustainable Chem.*, 2016, **2**, 28–33.
22 A. Brzęczek-Szafran, P. Więcek, M. Guzik and A. Chrobok, *RSC Adv.*, 2020, **10**, 18355–18359.
23 V. Zullo, A. Iuliano and L. Guazzelli, *Molecules*, 2021, **26**, 2052.
24 M. Petkovic, J. L. Ferguson, H. Q. N. Gunaratne, R. Ferreira, M. C. Leitão, K. R. Seddon, L. P. N. Rebelo and C. S. Pereira, *Green Chem.*, 2010, **12**, 643–649.
25 M. Sharma, D. Mondal, R. A. Sequeira, R. K. Talsaniya, D. A. Maru, K. Moradiya and K. Prasad, *J. Indian Chem. Soc.*, 2021, **98**, 100205.
26 J.-P. Mbakidi and S. Bouquillon, *J. Mol. Liq.*, 2018, **252**, 218–224.
27 S. Qian, J. D. Leah, S. Chatterjee, A. Soyemi, T. Szilvási and J. E. Bara, *J. Chem. Eng. Data*, 2022, **67**, 1905–1914.
28 R. M. Dias, L. C. G. Petrin, F. H. B. Sosa, A. M. da Costa Lopes, J. A. P. Coutinho and M. C. da Costa, *Ind. Eng. Chem. Res.*, 2020, **59**, 18193–18202.
29 P. Muthukuru, P. Krishnaraj, J. Rayadurgam and S. Rajasekhara Reddy, *New J. Chem.*, 2021, **45**, 20075–20090.
30 M. Vasiloiu, I. Cervenka, P. Gaertner, M. Weil, C. Schröder and K. Bica, *Tetrahedron: Asymmetry*, 2015, **26**, 1069–1082.
31 M. P. Pereira, R. de Souza Martins, M. A. L. de Oliveira and F. I. Bombonato, *RSC Adv.*, 2018, **8**, 23903–23913.
32 V. B. Saptal and B. M. Bhanage, *ChemSusChem*, 2017, **10**, 1145–1151.
33 S. Pavlovica, A. Zicmanis, E. Gzibovska, M. Klavins and P. Mekss, *Green Sustainable Chem.*, 2011, **1**, 103–110.
34 Q.-P. Liu, X.-D. Hou, N. Li and M.-H. Zong, *Green Chem.*, 2012, **14**, 304–307.
35 H. Xu, D. Chen and Z. Cui, *J. Surfactants Deterg.*, 2011, **14**, 167–172.
36 A. Leal-Duaso, S. Gracia-Barberan, J. A. Mayoral, J. Garcia and E. Pires, *Org. Process Res. Dev.*, 2020, **24**, 154–162.
37 B. Gaida and A. Brzęczek-Szafran, *Molecules*, 2020, **25**, 3285.
38 D.-J. Tao, Z. Cheng, F.-F. Chen, Z.-M. Li, N. Hu and X.-S. Chen, *J. Chem. Eng. Data*, 2013, **58**, 1542–1548.
39 Y. Cao and T. Mu, *Ind. Eng. Chem. Res.*, 2014, **53**, 8651–8664.
40 A. Leal-Duaso, P. Pérez, J. A. Mayoral, E. Pires and J. I. García, *Phys. Chem. Chem. Phys.*, 2017, **19**, 28302–28312.
41 A. Leal-Duaso, P. Pérez, J. A. Mayoral, J. I. García and E. Pires, *ACS Sustain. Chem. Eng.*, 2019, **7**, 13004–13014.
42 S. De Santis, G. Masci, F. Casciotta, R. Caminiti, E. Scarpellini, M. Campetella and L. Gontrani, *Phys. Chem. Chem. Phys.*, 2015, **17**, 20687–20698.
43 F. Fahri, K. Bacha, F. F. Chiki, J.-P. Mbakidi, S. Panda, S. Bouquillon and S. Fourmentin, *Environ. Chem. Lett.*, 2020, **18**, 1403–1411.
44 R. Alcalde, G. García, M. Atilhan and S. Aparicio, *Ind. Eng. Chem. Res.*, 2015, **54**, 10918–10924.
45 H. Jin, B. O'Hare, J. Dong, S. Arzhantsev, G. A. Baker, J. F. Wishart, A. J. Benesi and M. Maroncelli, *J. Phys. Chem. B*, 2008, **112**, 81–92.
46 A. P. Abbott, R. C. Harris and K. S. Ryder, *J. Phys. Chem. B*, 2007, **111**, 4910–4913.
47 Y. Arosa, C. D. Rodríguez Fernández, E. López Lago, A. Amigo, L. M. Varela, O. Cabeza and R. de la Fuente, *Opt. Mater.*, 2017, **73**, 647–657.
48 Y. Deng, P. Besse-Hoggan, P. Husson, M. Sancelme, A.-M. Delort, P. Stepnowski, M. Paszkiewicz, M. Gołębiowski and M. F. Costa Gomes, *Chemosphere*, 2012, **89**, 327–333.

49 U. Domańska, E. Bogel-Łukasik and R. Bogel-Łukasik, *Chem.–Eur. J.*, 2003, **9**, 3033–3041.
50 D. K. Maurya and T. P. A. Devasagayam, *Food Chem. Toxicol.*, 2010, **48**, 3369–3373.
51 J. H. Chen and C.-T. Ho, *J. Agric. Food Chem.*, 1997, **45**, 2374–2378.
52 H. Kikuzaki, M. Hisamoto, K. Hirose, K. Akiyama and H. Taniguchi, *J. Agric. Food Chem.*, 2002, **50**, 2161–2168.
53 X. Zhang, D. Lin, R. Jiang, H. Li, J. Wan and H. Li, *Oncol. Rep.*, 2016, **36**, 271–278.
54 F. Shakeel, M. M. Salem-Bekhit, N. Haq and N. A. Siddiqui, *J. Mol. Liq.*, 2017, **236**, 144–150.
55 W. Ji, Q. Meng, L. Ding, F. Wang, J. Dong, G. Zhou and B. Wang, *J. Mol. Liq.*, 2016, **224**, 1275–1281.
56 E. I. Alevizou and E. C. Voutsas, *J. Chem. Thermodyn.*, 2013, **62**, 69–78.
57 A. Leal-Duaso, J. A. Mayoral and E. Pires, *ACS Sustain. Chem. Eng.*, 2020, **8**, 13076–13084.